Crystal structure, spectroscopic studies and quantum mechanical calculations of 2-[((3-iodo-4-methyl)phenylimino)methyl]-5-nitrothiophene

ARTICLE *in* SPECTROCHIMICA ACTA PART A MOLECULAR AND BIOMOLECULAR SPECTROSCOPY · JANUARY 2015

Impact Factor: 2.35 · DOI: 10.1016/j.saa.2015.01.050 · Source: PubMed

3 AUTHORS, INCLUDING:

Gonca Özdemir Tarı
Ondokuz Mayıs Üniversitesi
9 PUBLICATIONS **9** CITATIONS
SEE PROFILE

Sümeyye Gümüş Uzun
Ondokuz Mayıs Üniversitesi
31 PUBLICATIONS **34** CITATIONS
SEE PROFILE

Spectrochimica Acta Part A: Molecular and Biomolecular Spectroscopy 141 (2015) 119–127

Contents lists available at ScienceDirect

Spectrochimica Acta Part A: Molecular and Biomolecular Spectroscopy

journal homepage: www.elsevier.com/locate/saa

Crystal structure, spectroscopic studies and quantum mechanical calculations of 2-[((3-iodo-4-methyl)phenylimino)methyl]-5-nitrothiophene

Gonca Özdemir Tarı [a,*], Sümeyye Gümüş [b], Erbil Ağar [b]

[a] Vezirköprü Vocational School, Ondokuz Mayıs University, 55200 Samsun, Turkey
[b] Department of Chemistry, Faculty of Arts & Science, Ondokuz Mayıs University, 55139 Kurupelit, Samsun, Turkey

HIGHLIGHTS

- The theoretical and experimental results of the title compound were compared.
- The NLO, MEP, FMOs and thermodynamic properties of the title compound were examined.
- The theoretical calculations were performed using B3LYP, B3PW91 and PBEPBE levels of 6-311G+(d,p) basis set.
- The energetic behaviors were calculated by Onsager and PCM models in the solvent media.

GRAPHICAL ABSTRACT

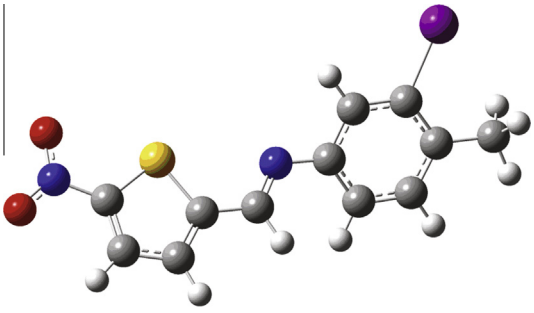

ARTICLE INFO

Article history:
Received 9 October 2014
Received in revised form 30 December 2014
Accepted 22 January 2015
Available online 30 January 2015

Keywords:
Schiff base
X-ray analysis
Density functional theory (DFT)
Non-linear optical properties (NLO)

ABSTRACT

The title compound, 2-[((3-iodo-4-methyl)phenylimino)methyl]-5-nitrothiophene, $C_{12}H_9O_2N_2I_1S_1$, was synthesized and characterized by IR, UV–Vis and single-crystal X-ray diffraction technique. The molecular structure was optimized at the B3LYP, B3PW91 and PBEPBE levels of the density functional method (DFT) with the 6-311G+(d,p) basis set. Using the TD-DFT method, the electronic absorption spectra of the title compound was computed in both the gas phase and ethanol solvent. The harmonic vibrational frequencies of the title compound were calculated using the same methods with the 6-311G+(d,p) basis set. The calculated results were compared with the experimental determination results of the compound. The energetic behavior such as the total energy, atomic charges, dipole moment of the title compound in solvent media were examined using the B3LYP, B3PW91 and PBEPBE methods with the 6-311G+(d,p) basis set by applying the Onsager and the polarizable continuum model (PCM). The molecular orbitals (FMOs) analysis, the molecular electrostatic potential map (MEP) and the nonlinear optical properties (NLO) for the title compound were obtained with the same levels of theory. And then thermodynamic properties for the title compound were obtained using the same methods with the 6-311G(d,p) basis set.

Introduction

Schiff's bases (azomethines, imines) belong to a widely used group of organic intermediates important for the production of certain chemical specialties, e.g. pharmaceuticals, or additives to rubber. A basic reaction synthesis involves an aromatic amine and aldehyde [1–3].

Schiff bases are used as starting materials in the synthesis of important drugs, such as antibiotics and antiallergic, antiphlogistic and antitumor substances [4–6]. In this paper, we have

* Corresponding author. Tel.: +90 3623121919.
E-mail address: gozdemir@omu.edu.tr (G. Özdemir Tarı).

http://dx.doi.org/10.1016/j.saa.2015.01.050
1386-1425/

characterized lots of physicochemical properties of the new thiophene containing compound. Over recent years, there has been an increasing interest in the chemistry of thiophenes because of their biological significance. Many of them have been widely investigated for therapeutic uses, especially as antifungal, antibacterial, anti-inflammatory, anticonvulsant, antiasthmatic and analgesic agents. They also were known to show anti-HIV, anti-proliferative, germicidal and D2 dopaminergic activities [7]. There are two characteristic properties of Schiff bases, viz. photochromism and thermochromism [8]. In general, Schiff bases display two possible tautomeric forms. The phenol-imine (OH) and the keto-amine (NH) forms. Depending on the tautomers, two types of intramolecular hydrogen bonds are observed in Schiff bases: O—H···N in phenol-imine [9,10] and N—H···O in keto-amine tautomers [11,12]. Another form of the Schiff base compounds is also known as zwitterion having an ionic intramolecular hydrogen bond (N^+—H···O^-) and this form is rarely seen in the solid state [13,14].

By means of increasing the development of computational chemistry in the past decade, the research of theoretical modeling of drug design, functional material design, etc. has become more mature than ever. Many important chemical and physical properties of biological and chemical systems can be predicted from the first principles by various computational techniques [15]. In recent years, density functional theory (DFT) has been a shooting star in theoretical modeling. The development of better and better exchange–correlation functionals made it possible to calculate many molecular properties with comparable accuracies to traditional correlated ab initio methods, with more favorable computational costs [16].

The most significant feature of the molecular structure, such as dipole moment, vibrational frequencies, electrostatic potentials, non-linear optical properties etc., are obtained by studies in the literature [17–20]. In the past decade, by increasing development of computational chemistry, density functional theory (DFT) has been used extensively to calculate a wide variety of molecular properties such as equilibrium structure, charge distribution, UV–Visible, FTIR and NMR spectra, and provided reliable results which are in accordance with experimental data [21].

In the present study, a new Schiff base, 2-[((3-iodo-4-methyl)phenylimino)methyl]-5-nitrothiophene was derived from 5-nitro-2-thiophene-carboxaldehyde and 3-iodo-4-methylaniline (Fig. 1). The crystal structure of the title compound was determined by IR, UV–Vis and the single-crystal diffraction technique. In addition the molecular structure and geometry, the MEP map, the FMOs and the NLO properties for the title compound at the B3LYP, B3PW91 and PBEPBE methods with the 6-311G+(d,p) basis set were performed. These studies are precious for providing insight into molecular properties of Schiff base compounds.

Experimental and theoretical methods

Synthesis

The compound 2-[((3-iodo-4-methyl)phenylimino)methyl]-5-nitrothiophene was prepared by reflux a mixture of a solution containing 5-nitro-2-thiophene-carboxaldehyde (0.0135 g 0.88 mmol) in 20 ml ethanol and a solution containing 3-iodo-4-methylaniline (0.0199 g 0.88 mmol) in 20 ml ethanol. The reaction mixture was stirred for 1 h under reflux. The crystals of 2-[((3-iodo-4-methyl)phenylimino)methyl]-5-nitrothiophene suitable for X-ray analysis were obtained from ethylalcohol by slow evaporation (yield %51; m.p 143–145 °C).

Instrumentation

The FT-IR spectrum of the title compound was recorded in the 4000–400 cm^{-1} region by a Shimadzu FTIR-8900 spectrophotometer using KBr pellets. Electronic absorption spectra were measured on a Unicam UV–Vis spectrophotometer in EtOH solvent.

X-ray crystallography

The crystal sample of size 0.68 × 0.43 × 0.24 mm^3 was prepared for the crystallographic studies. Reflection data were collected on an Stoe IPDS II diffractometer using MoKα radiation (λ = 0.71073 Å) at room temperature (296 K). The intensity symmetries indicate the monoclinic P21/c space group. A total of 9681 reflections with [2.09° < θ < 26.78°] were collected in the rotation made and cell parameters were determined using X-AREA software [22]. The structure was solved by direct methods using SHELXS 97 [23] and refined by a full-matrix least-squares method using the SHELXL-97 program [23], and then all non-hydrogen atoms were refined anisotropically. The molecular graphics were done using Ortep-3 for Windows [24] and PLATON [25]. The R_{int} value, which is obtained as the slightly high cause of the intensity data, was collected for the title structure generally weak, due to the poor quality of the crystal. The specification of data collection conditions and parameters of refinement process are given in Table 1.

Computational methods

The molecular geometry is directly taken from the X-ray diffraction experimental results without any constraints. All the computations were performed using the DFT method with the B3LYP [26,27], B3PW91 [28–30] and PBEPBE [31,32] levels of theory at 6-311G+(d,p) basis set as implemented in the Gaussian 03 W software [33]. The harmonic vibrational frequencies were calculated at the same levels of theory for the optimize structure and the vibrational band assignments were made using the GaussView molecular visualization program [16]. The electronic absorption spectra were calculated using the time-dependent density functional theory (TD-DFT) method [34–37]. Also, it was calculated in ethanol solution using the Polarizable Continuum Model (PCM) [38,39]. To investigate the reactive sites of the title compound the molecular electrostatic potential, $V(r)$, at a given point $r(x,y,z)$ in the vicinity of a molecule, is defined in terms of the interaction energy between the electrical charge generated by the molecule's electrons and nuclei and a positive test charge located at r. For the system studied the $V(r)$ values were calculated as described previously using the equation [40],

$$V(r) = \sum_A \frac{Z_A}{|R_A - r|} - \int \frac{\rho(r')}{|r' - r|} dr'$$

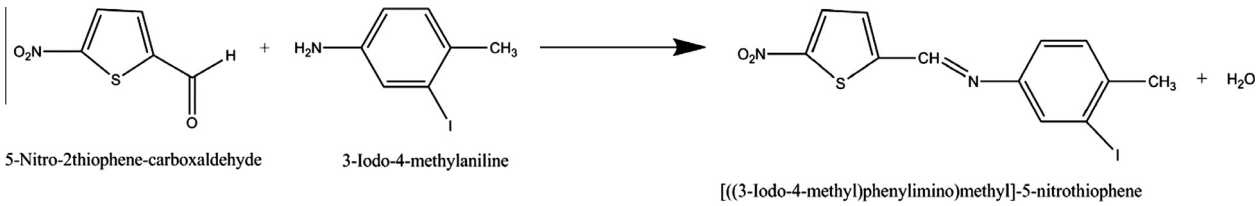

Fig. 1. 2-[((3-iodo-4-methyl)phenylimino)methyl]-5-nitrothiophene ($C_{12}H_9O_2N_2I_1S_1$).

Table 1
Crystal data and structure refinement parameters for the title compound.

Chemical formula	$C_{12}H_9O_2N_2I_1S_1$
Crystal color/shape	Yellow, prism
Formula weight	372.17
Crystal system	Monoclinic
Space group	P21/c
Unit cell parameters	a = 7.8044(4)
	b = 8.7804(3)
	c = 19.4997(10)
	β = 93.092(4)
Volume	1334.29 (11)
Density	1.853
Z	4
T_{min}, T_{max}	0.324, 0.571
θ_{min}, θ_{max}	2.1, 26.8
$F(000)$	720
Crystal size (mm^3)	0.68 × 0.43 × 0.24
Independent/observed reflections	2820/2367
R_{int}	0.1753
Diffractometer/measurement method	STOE IPDS II/w-scan
Refinement method	Full-matrix least-squares on F^2
Goodness of fit on F^2	1.063
R indices [$I > 2\sigma(I)$]	R_1 = 0.0731 wR_1 = 0.1107
R indices (all data)	R_2 = 0.0643 wR_2 = 0.1058

where Z_A is the charge of nucleus A, located at R_A, $\rho(r')$ is the electronic density function of the molecule, and r' is the dummy integration variable.

The linear polarizability properties of the title compound were obtained with the same levels at 6-311G+(d,p) basis set. The thermodynamic properties in the range of 100–500 K of the title compound were calculated using the same methods at the 6-311G(d,p) basis of vibrational analyses. In order to investigate the total energy, atomic charges, dipole moment (μ), chemical hardness (η) *and softness (S), electronegativity (χ), electron affinity (A) and ionization energy (I) of the title compound in solvent media, we also performed optimization calculations in three solvents (water, ethanol and chloroform) at the same levels using the Onsager [41] and PCM method. Thus, many important energetic properties of the title compound can be predicted by various computational techniques.*

3. Result and discussion

3.1. Description of the crystal structure

The title compound crystallizes in the monoclinic space group P21/c with Z = 4 in the unit cell. The crystal structure parameters of the title compound are a = 7.8044(4) Å, b = 8.7804(3) Å, c = 19.4997(10) Å and β = 93.092°. The asymmetric unit in the crystal structure contains only one molecule. In the title compound, $C_{12}H_9O_2N_2I_1S_1$, the thiophene ring and the benzene ring are essentially planar, while the dihedral angle between the two rings is 1.03°(21). The length of the N2=C5 double bond is 1.258 Å, which is slightly shorter than the standard 1.28 Å value, but it is consistent with related structures [1.269 Å and 1.282 Å, respectively] [42,43]. The N2—C6 bond distance is 1.416(5) Å, which is in sync with the corresponding bond lengths 1.419(3) Å and 1.422(2) Å, respectively [42,43]. The C1—S1 and C4—S1 distances are 1.716(4) Å and 1.709(4) Å, respectively. The values are very suitable standard for an C—S single bond character. And then, the distance is in sync with related compound 1.713(3) Å and 1.707(2) Å and the S···N2 distance is 3.043 Å in agreement with similar length in the related compound [42]. The imino group and nitro group are coplanar with the thiophene ring as can be shown by the S1—C4—N1—O2 and S1—C4—N1—O2 torsion angles are −7.5(6)° and −3.4(5)°, respectively.

Aromaticity is one of the most important concepts in organic chemistry [44]. The HOMA (harmonic oscillator model of aromaticity) value is a geometric indicator of aromaticity defined using the degree of bond-length alternation [45,46]. Aromaticities of both thiophene and phenyl rings were determined using the HOMA index using the following Eq. (1),

$$\mathrm{HOMA} = 1 - \left[\frac{\alpha}{n}\sum_{i=1}^{n}(R_i - R_{opt})^2\right]$$

where n is the number of bonds in the molecular fragments interested, α_i is the normalization constant (for C—C bonds α = 257.7 and C—S bonds α = 94.04), for the system with all bonds equal to the optimal value R_{opt} (for C—C bonds R_{opt} = 1.388 Å; for C—S bonds R_{opt} = 1.677 Å), R_i stands for a running bond length [46]. The HOMA indexes in the range of 0.900–0.990 or 0.500–0.800 show that the rings are aromatic or the non-aromatic, respectively [47,48]. The calculated HOMA index of C6—C11 benzene ring is 0.981 and C1—S1 thiophene ring is 0.870. These results show that the rings have aromatic character.

Thermochromism or photochromism depends on the planarity or non-planarity of the molecule, respectively. The molecular geometry of the title compound is almost planar with the rings of 1.03°(21). The title compound displays thermochromic properties because of the value of the dihedral angle. The crystal structure is stabilized by intermolecular C—H···O hydrogen bond (Fig. S1, Supporting Information).

One of the hydrogen bonds is between the C5—H5···O2^{i} hydrogen bond (symmetry code: $-1+x,y,z$), whereas the other is between the C12—H12B···O1^{i} hydrogen bond (symmetry code: $-1+x,3/2-y,1/2+z$). Moreover the π–π stacking interactions between the thiophene rings with a centroid–centroid distance of 3.7647 Å [Cg(1) is the centroid of the C1—C4/S1 ring (symmetry code:$1-x,1-y,-z$)]. These are interconnected by weak N—O···π interactions [N1—O2···Cg(2); Cg(2) is the centroid of the C6—C11 phenyl ring]. Details of these bonds and interactions are given in Table S1 (Supporting Information).

3.2. Theoretical structure

The optimized parameters of the title compound have been obtained using the B3LYP, B3PW91 and PBEPBE methods with the 6-311G+(d,p) basis set. These results are compared in Table S2 (Supporting Information). As can be seen in the Table S2; the experimental geometrical parameters show satisfactory agreement with the theoretical results. The C5—N2—C6—C7 and C5—N2—C6—C11 torsion angles are −172.2° and 8.0°, respectively. These torsion angles have been calculated at −150.8° and 31.45°; −148.6° and 33.79°; −151.1° and 31.39° for the B3LYP, B3PW91 and PBEPBE methods at the 6-311G+(d,p) level, respectively. The dihedral angle between the thiophene ring (S1—C4) and the benzene ring (C6—C11) is 1.03(21)° for X-ray, whereas the dihedral angle has been calculated at 33.29°, 34.92°, 32.89° for the B3LYP, B3PW91 and PBEPBE methods at the 6-311G+(d,p) level, respectively.

As can be seen from the dihedral angle between the rings and optimized parameters, most of the calculated parameters are slightly different from the experimental ones. It can be noted that the experimental results depend on the solid state, whereas the calculated results depend on the isolated gaseous phase. Thus, the most of the optimized bond lengths are slightly longer than the experimental values. In the solid state, the existence of the crystal field along with the inter-molecular interactions have connected with the molecules together, which result in the differences of bond parameters between the calculated and experimental values [49].

The maximum differences between the experimental values and those obtained from the theoretical calculations are 0.029 Å,

0.022 Å and 0.037 Å for bond distances and 1.893°, 2.029° and 2.152° for bond angles for B3LYP, B3PW31 and PBEBPE methods with the 6-311G+(d,p) basis set, respectively. According to these results, it can be deduced that for the title compound, the biggest differences of bond distances and bond angles mainly occur in the groups involved in the hydrogen bonds.

A logical method for globally comparing the structure obtained with the theoretical calculation is by superimposing the molecular skeleton with that obtained from X-ray diffraction (Fig. S2, Supporting Information). In order to compare the theoretical results with the experimental values, root mean square error (RMSE) is used. The computed RMSE values are 0.375, 0.383 and 0.412 Å for B3LYP, B3PW91 and PBEPBE methods with the 6-311G+(d,p) basis set, respectively. According to the obtained values, it may be concluded that the B3PW91 and PBEPBE calculations are the revaluation of the bond distances and angles of the title compound, while the B3LYP method is better in predicting the geometry of the title compound. On the other hand, these calculated RMSE values are slightly large. These large values can be explained by theoretical calculations which belong to the gas phase.

In addition, in order to evaluate the solvent effect on the geometric parameters of the title compound, we have carried out calculations in different solvents (chloroform, ethanol and water) with the B3LYP, B3PW91 and PBEPBE methods at the 6-311G+(d,p) level using the PCM model (Table S2 (Supporting Information)). When the experimental and theoretical structures are compared the obtained RMSE values are 0.381 Å for chloroform, 0.403 Å for ethanol and 0.392 Å. for water for the B3LYP; 0.397 Å for chloroform, 0.408 Å for ethanol and Å 0.415 for water for the B3PW91; 0.414 Å for chloroform, 0.419 Å for ethanol and 0.421 Å for water for the PBEBPE method; respectively. According to these results, it has been found that most of the optimized parameters are slightly larger than the experimental results, due to the theoretical calculations of isolated molecules in gas phase and experimental results of molecules in solid state. It is also observed that the calculated optimized parameters at the B3LYP method are closer to the experimental parameters than the B3PW91 and PBEPBE methods. It is observed that both the optimized parameters and the computed other parameters of the title compound increased at higher level of theory with higher polarity of the solvent.

The Mulliken atomic charges for the non-H atoms of the title compound was calculated at the B3LYP, B3PW91 and PBEPBE methods at the 6-311G+(d,p) level in gas-phase, and the results are given in Table S3 (Supporting Information). In addition, to investigate the solvent effect, the atomic charge distributions of the title compound, were calculated in different solvents (chloroform, ethanol and water) at the same levels using the PCM method, and the results are compared in Table S3 (Supporting Information). As can be seen from Table S3, the atomic charges increase with increasing the polarity of the solvent. The negative charges are delocalized in O1, O2 and N1 atoms. The positive charges are observed for hydrogen atoms connected with carbon atoms. It can be deduced that, these atoms are more negatively charged except N1 and it may cause the greater electronegative character of oxygen atoms (O1 and O2) and this situation is revealed stabilized by intermolecular hydrogen bond.

3.3. IR spectroscopy

The harmonic vibrational frequencies were calculated for the optimized structures at the B3LYP, B3PW91 and PBEPBE levels of theory with 6-311G+(d,p) basis set (Fig. S3, Supporting Information). The obtained frequencies were scaled by 0.9652 at B3LYP/6-311G+(d,p) level, 0.9542 at B3PW91/6-311G+(d,p) level, respectively [50]. It is reasonable to use a scale factor of 0.99 for the PBEPBE/6-311G+(d,p) as well. Some experimental and calculated IR assignments were compared and listed in Table 2.

Some characteristic bands of the stretching vibrations of the C—S, C—N, C=N, N—O_2, C—H, C=C groups were observed.

Thiophene C—S stretching is observed at 775 cm^{-1} in the free ligand. In all complexes, this band appears at lower frequencies in 728–771 cm^{-1} region, confirming the involvement of the thiophene sulfur in complex formation [51]. The C—S stretching vibration was seen at 734 cm^{-1} for experimentally and calculated at 651–680, 657–683 and 658–680 cm^{-1} for the B3LYP, B3PW91 and PBEBPE methods with the 6-311+G(d,p) basis set, respectively. The C—S stretching vibration is in agreement with the literature value 695 cm^{-1} [52].

The nitro group stretching vibration was observed at 1556 cm^{-1} for experimental that was calculated at 1522, 1545 and 1484 cm^{-1} for the B3LYP, B3PW91 and PBEBPE methods with the 6-311+G(d,p) basis set. The values are coherent with the literature value 1537 cm^{-1} [52].

The strong C—N stretching vibration was observed at 1337 cm^{-1} experimentally and calculated at 1307, 1321 and 1282 cm^{-1} for the B3LYP, B3PW91 and PBEBPE methods with the 6-311+G(d,p) basis set. This strong C—N stretching value is in good agreement with the related compounds [52,53]. The characteristic region of 1600–1700 cm^{-1} can be used to identify the proton transfer of Schiff bases. The strong absorption band at 1516 cm^{-1} in the IR experimental spectrum is due to the stretching vibrational of C=N. This band has been calculated at 1609, 1607 and 1595 cm^{-1} for the B3LYP, B3PW91 and PBEBPE methods with the 6-311+G(d,p) basis set. The band value is in good agreement with the corresponding band values 1608.7, 1620, 1623 cm^{-1}, respectively [54–56]. The benzene ring modes predominantly involve C=C bonds and vibrational frequency is associated with the C=C stretching modes of the carbon skeleton [57]. The absorption band located at 1542 cm^{-1} region is belongs to the aromatic C=C stretching in the experimental spectrum. The same bands have been calculated at 1502–1561, 1448–1519 and 1504–1549 cm^{-1} for the B3LYP, B3PW91 and PBEBPE methods with the 6-311+G(d,p) basis set. The values are in good agreement with the literature, at 1520–1581 and 1543–1565 cm^{-1}, respectively [53–56]. The weak bands in the range 3097–2927 cm^{-1} correspond to the asymmetric and symmetric stretching vibrations of aromatic CH bands, and were calculated at 2922–3126, 2898–3099 and 2917–3141 cm^{-1} for the B3LYP, B3PW91 and PBEBPE methods with the 6-311+G(d,p) basis set. These bands in the range are good agreement with the literature at 2900–3150 cm^{-1}, 3062–3021 cm^{-1}, 3033–3000 cm^{-1}, respectively [54,55]. Consequently,

Table 2
Comparison of the experimental and calculated vibrational frequencies (cm^{-1}).

Assignments[a]	Experimental IR	Calculated/6-311G+(d,p)		
		B3LYP	B3PW91	PBEPBE
υ(C—S)	734	651–680	657–683	658–680
υ(C—N)	1337	1307	1321	1282
υ(C=N)	1516	1609	1607	1595
$\upsilon_{thiophene}$(C=C)	1491	1420	1502	1503
$\upsilon_{benzene}$(C=C)	1542	1521	1518	1514
υ_{methyl}(C—H)	2927	2923–3001	2897–2984	2935–3026
γ_{methyl}(C—H)	–	1428	1410	1408
α_{methyl}(C—H)	–	1437	1344	1418
$\upsilon_{benzene}$(C—H)	3097	3053–3074	3027–3065	3066–3106
$\gamma_{benzene}$(C—H)	–	1457	1448	1450
$\upsilon_{thiophene}$(C—H)	3435	3092–3126	3067–3099	3108–3140
$\alpha_{thiophene}$(C—H)	–	1016	1006	1008
$\omega_{thiophene}$(C—H)	–	894	880	872
$\upsilon(NO_2)$	1556	1522	1545	1484

[a] υ, stretching; γ, rocking; α, scissoring; ω, wagging.

the scaled calculated theoretically values of the stretching vibration modes show good agreement with the experimental values, and also the assignments stretching modes decrease with the higher level of theory.

3.4. Electronic absorption spectra

The UV–Vis electronic spectra of the title compound in ethanol were recorded within 200–600 nm range at room temperature. Time-dependent density functional theory (TD-DFT) method is used to calculate the UV–Visible spectrum. In addition, electronic absorption spectra were calculated using the TD-DFT method based on the B3LYP, B3PW91 and PBEBPE methods with the 6-311G+(d,p) basis set optimized structure in the gas phase and ethanol solvent using the PCM model. Comparing these values with the corresponding experimental values, TD-DFT method for both in the gas phase and solvent media is useful to predict UV–Vis spectrum (Fig. 2).

Usually, in the UV–Vis spectrum of Schiff base compounds at 300–400 nm range indicates the excitation of electrons of C=N group. According to the experimental absorption spectrum, the molecule exhibits two absorption bands which were observed at 332 (log ε = 4.22) and 380 (log ε = 4.27) nm in EtOH. While one is the maximum absorption band at 380 nm which can be assigned to n → π^* transition within azomethine group, the other is the absorption band at 332 nm arising $\pi \rightarrow \pi^*$ transitions of the thiophene and benzene rings.

According to the TD-DFT calculated UV–Vis spectrum of the title compound absorption bands were observed at 442.11, 409.58 and 353.44 nm in gas phase. It can be seen that these values correspond to the experimental absorption ones. The PCM calculations reveal that the calculated absorption bands have slight red shifts with values of 477.03, 428.04 and 360.70 nm when compared with the gas-phase calculations of TD-DFT. The reason for this red shift is the solvent effect which can affect the geometry and electronic structure as well as the properties of the molecule as the solvent effects induce the lower energy of the molecules, and generate more significant red shift for absorption bands [58]. These values occured from HOMO → LUMO and HOMO-3 → LUMO HOMO-1 → LUMO transition and from HOMO-2 → LUMO transition, respectively. The same absorption bands were obtained at 477.03, 428.04 and 360.70 nm using the PCM model in ethanol solvent, and conform with the transitions from the HOMO → LUMO, HOMO-1 → LUMO and from HOMO-2 → LUMO, respectively. In addition, electronic absorption spectra were calculated using the TD-DFT method based on the B3PW91 and PBEBPE methods with the 6-311G+(d,p) basis set optimized structure in the gas phase and ethanol solvent using the PCM model. The comparative values of absorption spectra for three sets are presented in Table 3. According to Table 3, computed absorption spectra at higher level of theory with higher basis set are larger than the experimental absorption spectra.

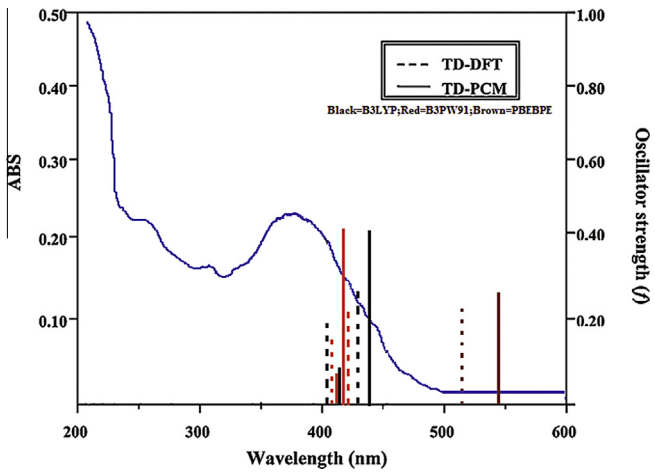

Fig. 2. UV–Vis absorption spectrum of the title compound in ethanol solvent and comparison of calculated transitions in gas phase and ethanol solvent with the experimental spectrum.

3.5. Frontier molecular orbitals analysis

The highest occupied molecular orbitals (HOMOs) and lowest-lying unoccupied molecular orbitals (LUMOs) are named called frontier molecular orbitals (FMOs). The FMOs play an important role in the electric and optical properties, as well as in UV–Vis spectra and chemical reactions [59]. The energy gap between the HOMO and LUMO is very important in determining the chemical activity of the molecule. A small HOMO–LUMO energy gap implies low kinetic stability, because it is energetically favorable to add electrons to a low-lying LUMO and to receive electrons from a high-lying HOMO [17,60–62]. The hardness is the energy gap between the two frontier orbitals. A hard molecule has a large HOMO–LUMO gap. Chemical hardness is a useful concept for understanding the behavior of chemical systems [63]. The energy levels of the HOMO-1, HOMO, LUMO and LUMO + 1 orbitals were computed at the B3LYP/6-311+G(d,p) level for the title compound in gas phase (Fig. S4, Supporting Information). As seen from Fig. S4, in the HUMO-1 and LUMO electrons are mainly delocalized on the thiophene ring and HOMO and LUMO + 1 electrons are delocalized on the whole structure. Molecular orbital coefficients analyses based on optimized geometry indicate that, for the title compound, the FMOs are mainly composed of p-atomic orbitals, so the aforementioned electronic transitions are mainly derived from the contribution of bands n → p^* and p → p^*.

Both the HOMOs and the LUMOs are mostly the π-antibonding type orbitals. As can be clearly seen from the Fig. S4 (Supporting Information), LUMO and HOMO-1 electrons are mainly delocalized on the thiophene ring and the HOMO and LUMO + 1 electrons are delocalized on the whole molecule. Electronegativity describes the tendency to attract the electrons of a bond. Electron affinity is defined as the ability of an atom to form an electron. The ionization energy of describes the minimum amount of energy required to remove an electron from the atom in the gaseous state [64]. The electron affinity and ionization potential are used to estimate the energy barrier of the electrons. The value of the energy barrier between the HOMO and LUMO is 3.164 eV, value of chemical hardness and softness are 1.582 and 0.315 eV for title compound in gas phase, respectively. In addition; total and FMOs energies, dipole moment (μ), electronegativity (χ), electron affinity (A), ionization energy (I), chemical hardness (η) and chemical softness (S) for the title compound at the B3LYP, B3PW91 and PBEPBE methods with the 6-311+G(d,p) basis set were calculated by Onsager and PCM models in different solvent media. The calculated results are given in Table 4.

As can be seen in Table 4, the obtained total molecular energy, the energy between gas phase and solvent media (ΔE) and the chemical hardness and softness of the title compound also decrease with the increasing polarity of the solvent. The dipole moments calculated by the Onsager method are larger than those of the PCM method in the different solvent. The dipole moments obtained from the two methods increase with the increasing of the solvent polarity. Solvent effects improve the charge delocalized in the molecules, therefore, inducing the dipole moments are to be raised. Ground state dipole moments are an important factor in measuring the solvent effect, a large ground-state dipole moment gives rise to strong solvent polarity effects [20,65,66].

Table 3
Experimental and calculated transitions of the title compound in various methods.

	Gas				Ethanol			
	λ	f	E	MO	λ	f	E	MO
B3LYP	442.11	0.2782	2.8044	HOMO → LUMO	477.03	0.4112	2.5991	HOMO → LUMO
	409.58	0.1518	3.0271	HOMO-3 → LUMO HOMO-1 → LUMO	428.04	0.0892	2.8966	HOMO-1 → LUMO
	353.44	0.0055	3.5080	HOMO-2 → LUMO	360.70	0.0174	3.4373	HOMO-2 → LUMO
B3PW91	434.81	0.2860	2.8515	HOMO-3 → LUMO HOMO → LUMO	465.23	0.4127	2.6650	HOMO → LUMO
	402.15	0.1283	3.0830	HOMO-3 → LUMO HOMO-1 → LUMO	415.96	0.0748	2.9807	HOMO-1 → LUMO
	346.17	0.0077	3.5816	HOMO-2 → LUMO	351.04	0.0464	3.5319	HOMO-3 → LUMO HOMO-2 → LUMO
PBEPBE	614.43	0.0419	2.0179	HOMO-1 → LUMO HOMO → LUMO	663.41	0.0937	1.8689	HOMO-1 → LUMO HOMO → LUMO
	533.14	0.2118	2.3256	HOMO-3 → LUMO HOMO-1 → LUMO HOMO → LUMO	584.54	0.2125	2.1211	HOMO-3 → LUMO HOMO-1 → LUMO HOMO → LUMO
	504.84	0.0069	2.4559	HOMO-2 → LUMO	526.82	0.0040	2.3535	HOMO-2 → LUMO

λ: wavelenth (nm); f: oscillator strength; E: excitation energy (eV); MO: molecular orbital.

Table 4
The calculated total molecular energies (Hartree), dipole moment (Debye), frontier orbital energies (eV), electronegativity (eV), hardness (eV) and softness (eV^{-1}) for the title compound using the B3LYP, B3PW91 and PBEPBE methods with the 6-311++G(d,p) basis set.

	ε	E_{TOTAL}	μ	I	A	ΔE	χ	η	S
B3LYP	ε = 1	−8011.085	6.9891	6.634	3.469		5.051	1.582	0.315
ONSAGER	ε = 4.9	−8011.086	7.5595	6.604	3.532	2.625	5.068	1.536	0.325
	ε = 24.55	−8011.086	7.7560	6.593	3.556	3.413	5.074	1.518	0.329
	ε = 78.39	−8011.086	7.7944	6.590	3.561	3.675	5.076	1.514	0.330
PCM	ε = 4.9	−8011.098	8.7787	6.481	3.464	34.394	4.972	1.508	0.331
	ε = 24.55	−8011.103	9.5291	6.451	3.474	48.571	4.963	1.488	0.335
	ε = 78.39	−8011.105	9.6962	6.443	3.477	52.247	4.960	1.483	0.337
B3PW91	ε = 1	−8010.851	6.8379	6.675	3.453		5.064	1.610	0.310
ONSAGER	ε = 4.9	−8010.852	7.5654	6.636	3.534	3.413	5.085	1.551	0.322
	ε = 24.55	−8010.853	7.8284	6.620	3.567	4.725	5.093	1.526	0.327
	ε = 78.39	−8010.853	7.8802	6.617	3.572	4.988	5.095	1.522	0.328
PCM	ε = 4.9	−8010.864	8.5739	6.538	3.450	34.394	4.994	1.544	0.323
	ε = 24.55	−8010.870	9.3047	6.514	3.461	48.309	4.987	1.526	0.327
	ε = 78.39	−8010.871	9.4714	6.509	3.461	51.984	4.985	1.523	0.328
PBEPBE	ε = 1	−8009.465	6.9371	5.910	4.051		4.981	0.929	0.538
ONSAGER	ε = 4.9	−8009.466	7.7081	5.880	4.119	3.150	5.000	0.880	0.567
	ε = 24.55	−8009.466	7.9883	5.869	4.147	4.200	5.008	0.874	0.571
	ε = 78.39	−8009.466	8.0444	5.866	4.152	4.463	5.009	0.857	0.583
PCM	ε = 4.9	−8009.478	8.8904	5.768	4.043	33.868	4.906	0.862	0.579
	ε = 24.55	−8009.483	9.6989	5.744	4.054	47.259	4.899	0.844	0.591
	ε = 78.39	−8009.484	9.8794	5.738	4.054	51.197	4.896	0.842	0.593

$\Delta E = E_{Solvation} - E_{Gas}$, $I = -E_{HOMO}$, $A = -E_{LUMO}$, $\chi = \frac{I+A}{2}$, $\eta = \frac{I-A}{2}$, $S = \frac{1}{2\eta}$.

3.6. Molecular electrostatic potential

Investigating the molecular electrostatic potential (MEP) generated in the space around a molecule by the charge distribution is very helpful in understanding the sites for electrophilic attacks and nucleophilic reactions for the study of biological recognition processes [67] and hydrogen bonding interactions [68]. Being a real physical property, $V(r)$ can be determined experimentally by diffraction or by computational methods [69]. To predict reactive sites of electrophilic and nucleophilic attack for the investigated molecule MEP map of the title molecule was calculated at the B3LYP/6-311+G(d,p) optimized geometry. The negative (red and yellow) regions of the MEP are related to electrophilic reactivity and the positive (blue) regions to nucleophilic reactivity (see Fig. 3). As can be seen in Fig. 3, there are several possible sites of electrophilic attack.

Negative electrostatic potential regions are mainly localized over the O1, O2, N1 and N2 atoms, and then $V(r)$ values are −0.044, −0.046, −0.047, −0.024 a.u., respectively. However, positive electrostatic potential regions are localized on the C2—H2, C3—H3, C5—H5 atoms. The $V(r)$ values are 0.037, 0.031, 0.035 a.u., respectively. According to these calculated results, the MEP map shows that the negative potential sites are on oxygen and nitrogen atoms and the positive potential sites are around the hydrogen atoms. In addition, the MEP is best suited for identifying sites for intra- and intermolecular interactions [70]. So, the MEP map confirms the existence of the intermolecular C5—H5···O2 interactions.

3.6. Nonlinear optical effects

The Schiff base compounds have been also under investigation during last years because of their potential applicability in optical communications and many of them have NLO behavior [71–73].

Nonlinear optical (NLO) effects arise from the interactions electromagnetic fields in various media to produce new fields altered

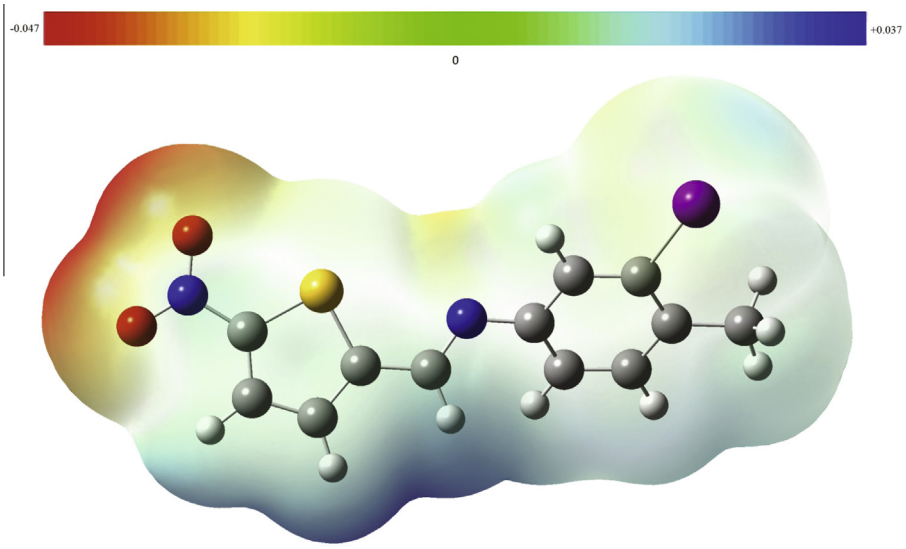

Fig. 3. Molecular electrostatic potential map calculated at B3LYP/6-311+G(d,p) level.

Table 5
The calculated values of μ (D), α (Å^3), $\Delta\alpha$ (Å^3) and β ($\times 10^{-30}$ esu) for the title compound in different solvents.

		Gas phase (ε = 1)	Chloroform (ε = 4.9)	Ethanol (ε = 24.55)	Water (ε = 78.39)
B3LYP	μ	2.749	3.453	3.749	3.814
	α	38.711	50.148	54.940	56.106
	$\Delta\alpha$	119.940	153.867	165.340	167.869
	β	74.802	186.913	242.344	254.964
B3PW91	μ	2.690	3.373	3.660	3.726
	α	38.020	49.046	53.637	54.760
	$\Delta\alpha$	117.612	149.867	160.550	162.902
	β	69.122	167.465	214.211	224.774
PBEPBE	μ	2.729	3.498	3.816	3.887
	α	42.410	56.658	62.712	64.177
	$\Delta\alpha$	138.115	186.166	203.733	207.664
	β	120.649	338.964	471.612	502.604

in phase, frequency, amplitude other propagation characteristics from the incident fields [74]. The organic molecules which contain both conjugated bonds and acceptor group on one side and a donor group on the other side are known as nonlinear optical (NLO) materials [75]. NLO is at the forefront of current research because of its importance in providing the key functions of frequency shifting, optical modulation, optical switching, optical logic, and optical memory for the emerging technologies in areas such as telecommunications, signal processing and optical interconnections [76–79].

Nonlinear optical (NLO) materials play a major role in nonlinear optics and in particular they have a great impact on information technology and industrial applications. In the last decade, however, this effort has also brought its fruits in applied aspects of nonlinear optics. This can be essentially traced to the improvement of the performances of the NLO materials. There has been a growing interest in crystal growth process, particularly, in view of the increasing demand for materials for technological applications [80–82].

To investigate the effects of different solvent on the NLO properties of the title compound, the dipole moment (μ), linear polarizability (α), anisotropy of the polarizability ($\Delta\alpha$) and first hyperpolarizability (β) were calculated in solvent media with the B3LYP, B3PW91 and PBEPBE methods at the 6-311G+(d,p) level using PCM model. The calculated values of μ, α, $\Delta\alpha$ and β for the title compound are listed in Table 5. As can be seen from the Table 5, dipole moment, linear polarizability, anisotropy of the polarizability and first hyperpolarizability of the title compound were raised with the polarity of the solvent and the high levels of theory.

The electronegativite of the halogens decreases as you go down the group. Halogens include the elements of the highest electronegativite, as the iodine containing the title compound is much greater than the expected β value.

On the other hand, the wavelength obtained by UV–Vis spectra analysis can be helpful in planning the synthesis of the promising NLO materials [83]. The maximum absorption wavelengths of the synthesized compounds found shorter than 400 nm show that such compounds might have non-zero rather high first hyperpolarizabilities [84]. The maximum absorption wavelengths of the title compound obtained shorter than 400 nm show that such a compound might have rather high β value.

As can be seen, the obtained energy gaps between HOMO–LUMO of the title compound are 3.164, 3.22 and 1.858 eV for the B3LYP, B3PW91 and PBEPBE methods with the 6-311G+(d,p) basis set, respectively. The calculated values of β are 74.802, 69.122 and 120.649 $\times$ 10^{-30} esu, respectively. As expected, the high values of β corresponds to the low HOMO–LUMO gap. The value for these compounds are an inverse relationship the energy gap between HOMO and LUMO for its. As the HOMO–LUMO energy gap of the related compounds are decreased the β values increased [17,20,53,85]. These values of the title compound are greater than

those of the urea [74] and theoretically the β values of the title compound is about 20 times for the B3LYP, 18 times for the B3PW91 and 32 times for the PBEPBE magnitude of urea. These results may be a potential applicant in the development of NLO materials.

3.7. Thermodynamic properties

The standard thermodynamic functions enthalpy (H_m^0), entropy (S_m^0) and heat capacity ($C_{p,m}^0$) for the title compound were calculated using the B3LYP, B3PW91 and PBEPBE methods with the 6-311G(d,p) basis of vibrational analysis and statistical thermodynamics. The vibrational frequencies were calculated at the same levels of theory for the optimized structures and the obtained frequencies were scaled by 0.9669 at the B3LYP/6-311G(d,p) level, 0.9631 at the B3PW91/6-311G(d,p) level and 0.9910 at the PBEPBE/6-311G(d,p) level, respectively [86].

The heat capacities, the enthalpies and the entropies were obtained at different temperatures going from 100.00 to 500.00 K, and correlation equations are listed in the Table S4 (Supporting Information). According to the calculations, it was obtained that the entropy increases otherwise the enthalpy and the heat capacity remain stable, when the pressure is increased at constant temperature. Boyle's Law explain how the pressure of a molecule tends to decrease as to the volume of a molecule increases in Table S4 (Supporting Information). Boyle's Law describes the volume and pressure of a gas inversely related [87].

The standard heat capacities, enthalpies and entropies increase because the intensities of the molecular vibration increase with the increasing temperature. The correlations between the thermodynamic functions and temperatures are as follows:

B3LYP

$$H_m^0 = -0.63268 + 0.01464\ T + 8.2228 \times 10^{-5}\ T^2\ (R^2 = 0.99952).$$
$$C_{p,m}^0 = 4.3137 + 0.21283\ T - 7.77983 \times 10^{-5}\ T^2\ (R^2 = 0.99617).$$
$$S_m^0 = 57.18643 + 0.3024\ T - 1.16407 \times 10^{-4}\ T^2\ (R^2 = 0.99704).$$

B3PW91

$$H_m^0 = -0.39156 + 0.01393\ T + 7.56972 \times 10^{-5}\ T^2\ (R^2 = 0.99997).$$
$$C_{p,m}^0 = 7.39125 + 0.18818\ T - 6.43956 \times 10^{-5}\ T^2\ (R^2 = 0.99974).$$
$$S_m^0 = 62.07331 + 0.26267\ T - 9.73088 \times 10^{-5}\ T^2\ (R^2 = 0.99982).$$

PBEPBE

$$H_m^0 = -0.44449 + 0.01469\ T + 8.00426 \times 10^{-5}\ T^2\ (R^2 = 0.99997).$$
$$C_{p,m}^0 = 6.9849 + 0.20549\ T - 7.89936 \times 10^{-5}\ T^2\ (R^2 = 0.99967).$$
$$S_m^0 = 63.65629 + 0.27679\ T - 1.01661 \times 10^{-4}\ T^2\ (R^2 = 0.99985).$$

As a result, these equations will be helpful for studies like the title compound in the future.

Conclusions

The new Schiff base 2-[((3-iodo-4-methyl)phenylimino)methyl]-5-nitrothiophene has been studied using FT-IR, UV–Visible and X-ray crystallographic technique. The results of experimental studies are supported by some quantum mechanics calculations. The molecular structure and optimized geometry, the MEP map, the FMOs, the electronic absorption spectra, the harmonic vibrational frequencies and the NLO properties for the title compound have been calculated at the B3LYP, B3PW91 and PBEPBE methods with the 6-311 g+(d,p) polarized and diffused basis set. In addition, some theoretical calculations of the title compound were obtained by the same levels of theory in different solvent PCM method. Comparison between the calculated and experimental parameters shows that B3LYP method results are in good agreement with experimental values.

Vibrational frequencies are determined experimentally and compared with those obtained theoretically. And then, the computed UV–Vis spectra are compared with the experimental observations. These results show that the predicted FT-IR and UV–Vis spectra analyses are in good agreement with the experimental values. The NLO properties of the title compound were calculated in different solvent media. Similarly, the total energy, ionization potential and chemical hardness of the title compound were calculated in solvent media by the same methods. According to these values, the energetic properties of the title compound decrease with increasing the molecular polarity in medium. According to these values, the energetic properties of the title compound decreases with increasing the molecular polarity in medium.

The calculated NLO values increases with the polarity of the solvent. On the other hand, NLO properties for organic compounds are related to the electron absorption spectra. It has been obtained that the title compound has rather great β and λ values shorter than 400 nm. Also, the calculated NLO components are related to the electronegativite of the title compound. NLO properties of the title compound are much greater than those of urea [74]. Therefore, the title compound may be a potential applicant in the development of NLO materials. In addition, the MEP map gives information about the region with which the compound can have intermolecular interactions. The thermodynamic properties of the title compound were also obtained from constant temperature and pressure. Then, we hope this study will be helpful for the design and the synthesis of new materials like the title compound in the future.

Acknowledgement

I'm greatly thankful for the considerable contributions of my dear advisor Prof. Dr. Şamil Işık (pass away, may god bless his soul.).

Appendix A. Supplementary data

Supplementary data associated with this article can be found, in the online version, at http://dx.doi.org/10.1016/j.saa.2015.01.050.

References

[1] H. Schiff, Justus Liebigs Ann. Chem. 140 (1867) 93;
H. Schiff, Justus Liebigs Ann. Chem. 148 (1868) 330;
H. Schiff, Justus Liebigs Ann. Chem. 201 (1880) 355;
H. Schiff, Justus Liebigs Ann. Chem. 210 (1881) 119.
[2] E.H. Cordes, W.P. Jenks, J. Am. Chem. Soc. 84 (1962) 832.
[3] J. March, Advanced Organic Chemistry, Reactions, Mechanism and Structure, fourth ed., Wiley, New York, 1992. p. 986.
[4] D. Barton, W.D. Ollis, Comprehensive Organic Chemistry, Pergamon, Oxford, 1979.
[5] R.W. Layer, Chem. Rev. 63 (1963) 489–510.
[6] C.K. Ingold, Structure and Mechanism in Organic Chemistry, second ed., Cornell University Press, Ithaca, 1969.
[7] M. Mohareb, M. Sherif, M. Gaber, S. Ghabrial, I. Aziz, Heteroatom Chem. 15 (2004) 15.
[8] M.D. Cohen, G.M.J. Schmidt, S. Flavian, J. Chem. Soc. (1964) 2041
[9] G. Özdemir Tarı, Ş. Işık, Ramazan Özkan, A. Alaman Ağar, Acta Crystallogr. E67 (2011) o343–o344.
[10] Ç. Albayrak, B. Koşar, S. Demir, M. Odabaşoğlu, O. Büyükgüngör, J. Mol. Struct. 963 (2010) 211.
[11] H. Tanak, F. Erşahin, Y. Köysal, E. Ağar, Ş. Işık, M. Yavuz, J. Mol. Model. 15 (2009) 1281–1290.
[12] O. Şahin, Ç. Albayrak, M. Odabaşoğlu, O. Büyükgöngör, Acta Crystallogr. E61 (2005) o2859–o2861.
[13] G. Özdemir Tarı, H. Tanak, M. Macit, F. Erşahin, Ş. Işık, Acta Crystallogr. E66 (2010) o85.
[14] A. Trzesowska-Kruszynska, Stuct. Chem. 21 (2010) 131.
[15] Y. Zhang, Z.J. Guo, X.Z. You, J. Am. Chem. Soc. (2001) 9378–9387

[16] R. Dennigton II, T. Keith, J. Millam, GaussView, Version 4.1.2, Semichem Inc., Shawnee Mission, KS, 2007.
[17] S. Yazıcı, Ç. Albayrak, İ.E. Gümrükçüoğlu, İ. Şenel, O. Büyükgüngör, Spectrochim. Acta A 93 (2012) 208–213.
[18] Y. Bingöl Alpaslan, G. Alpaslan, A. Alaman Ağar, N. Ocak İskeleli, Emin Öztekin, J. Mol. Struct. 995 (2011) 58–65.
[19] E. İnkaya, M. Dinçer, E. Korkusuz, İ. Yıldırım, J. Mol. Struct. 1013 (2012) 67–74.
[20] Y. Köysal, H. Tanak, Spectrochim. Acta A 93 (2012) 106–115.
[21] W. Koch, M.C. Holthausen, A Chemist's Guide to Density Functional Theory, second ed., WILEY/VCH Verlag GmbH, Weinheim, 2001.
[22] Stoe & Cie, X-AREA (Version 1.18) and X-RED32 (Version 1.04). Stoe & Cie, Darmstadt, Germany, 2002.
[23] G.M. Sheldrick, SHELXS 97 and SHELXL 97, University of Göttingen, Germany, 1997.
[24] L.J. Farrugia, J. Appl. Crystallogr. 30 (1997) 565.
[25] A.L. Spek, Acta Crystallogr. D65 (2009) 148–155.
[26] A.D. Becke, J. Chem. Phys. 98 (2009) 5648.
[27] C. Lee, W.T. Yang, R.G. Parr, Phys. Rev. B 37 (1988) 785.
[28] A.D. Becke, Phys. Rev. A 38 (1988) 3098.
[29] J.P. Perdew, J.A. Chevary, S.H. Vosko, K.A. Jackson, M.R. Pederson, D.J. Singh, C. Fiolhais, Phys. Rev. B 48 (1993) 4978.
[30] J.P. Perdew, K. Burke, Y. Wang, Phys. Rev. B 54 (1996) 16533.
[31] J.P. Perdew, K. Burke, M. Ernzerhof, Phys. Rev. Lett. 77 (1996) 3865.
[32] J.P. Perdew, K. Burke, M. Ernzerhof, Phys. Rev. Lett. 78 (1997) 1396.
[33] M.J. Frisch, G.W. Trucks, H.B. Schlegel, G.E. Scuseria, M.A. Robb, J.R. Cheeseman, J.A. Montgomery Jr., T. Vreven, K.N. Kudin, J.C. Burant, J.M. Millam, S.S. Iyengar, J. Tomasi, V. Barone, B. Mennucci, M. Cossi, G. Scalmani, N. Rega, G.A. Petersson, H. Nakatsuji, M. Hada, M. Ehara, K. Toyota, R. Fukuda, J. Hasegawa, M. Ishida, T. Nakajima, Y. Honda, O. Kitao, H. Nakai, M. Klene, X. Li, J.E. Knox, H.P. Hratchian, J.B. Cross, V. Bakken, C. Adamo, J. Jaramillo, R. Gomperts, R.E. Stratmann, O. Yazyev, A.J. Austin, R. Cammi, C. Pomelli, J.W. Ochterski, P.Y. Ayala, K. Morokuma, G.A. Voth, P. Salvador, J.J. Dannenberg, V.G. Zakrzewski, S. Dapprich, A.D. Daniels, M.C. Strain, O. Farkas, D.K. Malick, A.D. Rabuck, K. Raghavachari, J.B. Foresman, J.V. Ortiz, Q. Cui, A.G. Baboul, S. Clifford, J. Cioslowski, B.B. Stefanov, G. Liu, A. Liashenko, P. Piskorz, I. Komaromi, R.L. Martin, D.J. Fox, T. Keith, M.A. Al-Laham, C.Y. Peng, A. Nanayakkara, M. Challacombe, P.M.W. Gill, B. Johnson, W. Chen, M.W. Wong, C. Gonzalez, J.A. Pople, Gaussian 03, Revision E.01, Gaussian Inc., Wallingford CT, 2004.
[34] E. Runge, E.K.U. Gross, Phys. Rev. Lett. 52 (1984) 997.
[35] R.E. Stratmann, G.E. Scuseria, M.J. Frisch, J. Chem. Phys. 109 (1988) 8218.
[36] R. Bauernschmitt, R. Ahlrichs, Chem. Phys. Lett. 256 (1996) 454.
[37] M.E. Casida, C. Jamorski, K.C. Casida, D.R. Salahub, J. Chem. Phys. 108 (1998) 4439.
[38] M. Cossi, N. Rega, G. Scalmani, V. Barone, J. Comput. Chem. 24 (2003) 669.
[39] J. Tomasi, B. Mennucci, R. Cammi, Chem. Rev. 105 (2005) 2999.
[40] P. Politzer, J.S. Murray, Theor. Chem. Acc. 108 (2002) 134.
[41] L. Onsager, J. Am. Chem. Soc. 58 (1936) 1486–1493.
[42] G. Özdemir Tarı, Ş. Işık, Acta Crystallogr. E68 (2012) o415.
[43] C. Kazak, M. Aygün, G. Turgut, M. Odabaşoğlu, S. Özbey, O. Büyükgüngör, Acta Crystallogr. C56 (2000) 1044.
[44] V.I. Minkin, M.N. Glukhovtsev, B.Y. Simkin, Aromaticity and Antiaromaticity, Wiley, New York, 1994.
[45] J. Kruszewski, T.M. Krygowski, Tetrahedron Lett. 13 (1972) 3839–3842.
[46] T.M. Krygowski, J. Chem. Inf. Comput. Sci. 33 (1993) 70–78.
[47] A. Filarowski, A. Koll, T. Glowiak, J. Chem. Soc. Perkin Trans. 2 (2002) 835–842.
[48] A. Filarowski, A. Kochel, M. Kluba, F.S. Kamounah, J. Phys. Org. Chem. 21 (2008) 939–944.
[49] F.F. Jian, P.S. Zhao, Z.S. Bai, L. Zhang, Struct. Chem. 16 (2005) 635.
[50] Y.Z. Song, A.F. Zhu, J.S. Lv, G.X. Gong, J.M. Xie, J.F. Zhou, Y. Ye, X.D. Zhong, Spectrochim. Acta Part A 73 (2009) 96–100.
[51] R.C. Maurya, P. Patel, Spectrosc. Lett. 32 (2) (1999) 213–236.
[52] H. Tanak, A. Alaman Ağar, O. Büyükgüngör, Spectrochim. Acta Part A 118 (2014) 672–682.
[53] G. Alpaslan, M. Macit, A. Erdönmez, O. Büyükgüngör, J. Mol. Struct. 1016 (2012) 22–29.
[54] H. Tanak, A. Ağar, M. Yavuz, J. Mol. Model. (2010) 577–587
[55] G. Alpaslan, M. Macit, A. Erdönmez, O. Büyükgüngör, J. Mol. Struct. (2011) 70–77
[56] B. Koşar, Ç. Albayrak, C.C. Ersanlı, M. Odabaşoğlu, O. Büyükgüngör, Spectrochim. Acta A 93 (2012) 1–9.
[57] A. Teimouri, A.N. Chermahini, K. Taban, H.A. Dabbagh, Spectrochim. Acta Part A 72 (2009) 369.
[58] Z.C. Rong, L.Z. Jiang, C.Y. Hong, C.H. Shan, Y. ZhiWu, Y.L. Hua, J. Mol. Struct. (Theochem) 899 (2009) 86.
[59] I. Fleming, Frontier Orbitals and Organic Chemical Reactions, Wiley, London, 1976.
[60] M.D. Diener, J.M. Alford, Nature 393 (1998) 668–671.
[61] S.H. Yang, C.L. Pettiette, J. Conceicao, O. Cheshnovsky, R.E. Smalley, Chem. Phys. Lett. 139 (1987) 233–238.
[62] H. Handschuh, G. Ganteför, B. Kessler, P.S. Bechthold, W. Eberhardt, Phys. Rev. Lett. 74 (1995) 1095–1098.
[63] R.G. Pearson, J. Chem. Sci. 117 (5) (2005) 369–377.
[64] P. Muller, Glossary of terms used in physical organic chemistry (IUPAC Recommendations), Pure Appl. Chem. 66 (5) (1994) 1077–1184.
[65] A. Masternak, G. Wenska, J. Milecki, B. Skalski, S. Franzen, J. Phys. Chem. 109 (2005) 759–766.
[66] Y. Le, J.F. Chen, M. Pu, Int. J. Pharm. 358 (2008) 214–218.
[67] P. Politzer, P.R. Laurence, K. Jayasuriya, Environ. Health Perspect. 61 (1985) 191–202.
[68] P. Politzer, P. Lane, Struct. Chem. 1 (1990) 159–164.
[70] P. Politzer, D.G. Truhlar, Chemical Applications of Atomic and Molecular Electrostatic Potentials, Plenum, New York, 1981.
[70] P. Politzer, M.C. Concha, J.S. Murray, Int. J. Quantum Chem. 80 (2000) 184.
[71] M. Jalali-Heravi, A.A. Khandar, I. Sheikshoaire, Spectrochim. Acta A 55 (1999) 2537.
[72] J.F. Nicoud, R.J. Twieg, in: D.S. Chemla, J. Zyss (Eds.), Nonlinear Optical Properties of Organic Molecules and Crystals, vol. 1, Academic Press, New York, 1987, p. 277 (Chap. II-3).
[73] M. Jalali-Heravi, A.A. Khandar, I. Sheikshoaire, Spectrochim. Acta A 56 (2000) 1575.
[74] Y.X. Sun, Q.L. Hao, W.X. Wei, Z.X. Yu, L.D. Lu, X. Wang, Y.S. Wang, J. Mol. Struct. Theochem 904 (2009) 74.
[75] C.H. Liu et al., DFT study on second-order nonlinear optical properties of a series of mono Schiff base M (II) (M = Ni, Pd, Pt) complexes, Chem. Phys. Lett. 429 (2006) 570.
[76] C. Andraud, T. Brotin, C. Garcia, F. Pelle, P. Goldner, B. Bigot, A. Collet, J. Am. Chem. Soc. 116 (1994) 2094.
[77] V.M. Geskin, C. Lambert, J.L. Bredas, J. Am. Chem. Soc. 125 (2003) 15651.
[78] M. Nakano, H. Fujita, M. Takahata, K. Yamaguchi, J. Am. Chem. Soc. 124 (2002) 9648.
[79] D. Sajan, H. Joe, V.S. Jayakumar, J. Zaleski, J. Mol. Struct. 785 (2006) 43.
[80] R.A. Laudise, in: R. Ueda, J.B. Millin (Eds.), Crystal Growth and Characterization, Holland Publishing Co., 1975.
[81] J.C. Brice, Crystal Growth Processes, Halsted Press, John Wiley and Sons, New York, 1986.
[82] H.S. Nalwa, S. Miyata, Nonlinear Optics of Organic Molecules and Polymers, CRC Press Inc., New York, 1996.
[83] S. Di Bella, I. Fragala, I. Ledoux, M.A. Diaz-Gacia, T.J. Marks, J. Am. Chem. Soc. 119 (1997) 9550–9557.
[84] Y. Zhou, Mater. Sci. Eng. B99 (2003) 593.
[85] H. Tanak, Comput. Theor. Chem. 967 (2011) 93–101.
[86] K.K. Irikura, R.D. Johnson III, R.N. Kacker, J. Phys. Chem. A 109 (2005) 8430–8437.
[87] J.B. West, J. Appl. Physiol. 87 (1999) 1543–1545.